

**DETC2005-84217**

**MODELING AND ALLEVIATING INSTABILITY IN A MEMS VERTICAL COMB DRIVE  
USING A PROGRESSIVE LINKAGE**

Jessica R. Bronson  
Mechanical and Aerospace Engineering  
University of Florida, Gainesville, FL  
jraeb@ufl.edu

Gloria J. Wiens  
Mechanical and Aerospace Engineering  
University of Florida, Gainesville, FL  
gwiens@ufl.edu

James J. Allen  
Microsystem Device Technologies  
Sandia National Laboratories, Albuquerque, NM  
jjallen@sandia.gov

**ABSTRACT**

Micro mirrors have emerged as key components for optical microelectromechanical system (MEMS) applications. Electrostatic vertical comb drives are attractive because they can be fabricated underneath the mirror, allowing for arrays with a high fill factor. Also, vertical comb drives are more easily controlled than parallel plate actuators, making them the better choice for analog scanning devices. The device presented in this paper is a one-degree of freedom vertical comb drive fabricated using Sandia National Laboratories SUMMiT™ five-level surface micromachining process. The electrostatic performance of the device is investigated using finite element analysis to determine the capacitance for a unit cell of the comb drive as the position of the device is varied. This information is then used to design a progressive linkage that will seek to alleviate or eliminate the effects of instability. The goal of this research is to develop an electrostatic model for the behavior of the vertical comb drive mirror and then use this to design a progressive-linkage that can delay or eliminate the pull-in instability.

**INTRODUCTION**

Micro mirrors have emerged as key components for optical microelectromechanical system (MEMS) applications. Electrostatic vertical comb drives are attractive because they can be fabricated underneath the mirror, allowing for arrays with a high fill factor. Vertical comb drives are also more easily controlled than parallel plate actuators, making them the better choice for analog scanning devices. However, electrostatic actuators suffer from an instability known as

‘pull-in’. Electrostatic pull-in occurs when the electrostatic force exceeds the mechanical restoring force of the device causing the actuator to abruptly move, or pull-in, to its final position. This behavior can be advantageous when designing a digital micro mirror in which only two stable positions are required. However, for devices that require a continuous motion over the full actuation range, such as micro mirrors for scanning applications, the actuator is limited by this instability [1-5]. Another phenomenon associated with this instability is that once the mirror has pulled-in, the voltage required to maintain that position is lower than the pull-in voltage. The mirror will not return from this position until the actuating voltage has been reduced below the holding-voltage. The result of this holding effect is hysteresis.

Other authors have studied the electrostatic pull-in phenomena and developed analytical models for predicting the location and the voltage of the pull-in [5]. It has also been shown that changing the device geometry can alter the instability point. However, in some applications, this may not be the best option, therefore it is important to consider alternative methods.

The device presented in this paper, depicted in Figure 1, is a micro mirror designed to operate with one-degree of freedom using a hidden vertical comb drive fabricated using Sandia National Laboratories SUMMiT™ five-level surface micromachining process. The electrostatic performance of the device is investigated using finite element analysis to determine the capacitance for a unit cell of the comb drive as the position of the device is varied. This information is then used to design a progressive linkage that will seek to alleviate

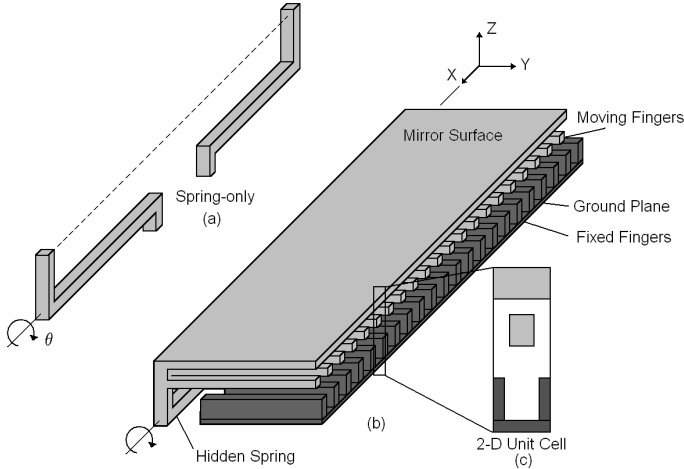


**Figure 1. Schematic of mirror with hidden vertical comb drive showing (a) the hidden spring by itself, (b) the full device, (c) and a 2-D cross-section view of a unit cell (figure not to scale).**

or eliminate the effects of instability. The goal of this research is to develop an electrostatic model for the behavior of the vertical comb drive mirror and then use this to design a progressive-linkage that can affect the pull-in angle.

The progressive linkage design and analysis is based on that of a four-bar mechanism that will provide nonlinear restoring torque to the vertical comb drive device. Previous work at developing a MEMS four-bar mechanism for motion amplification was conducted by Lee, et al [6]. That device was created by bulk etching into single crystal silicon. The device presented here is created within the SUMMIT™ V micromachining process.

## NOMENCLATURE

$T_e$ , electrostatic torque  
 $N$ , number of unit cells  
 $C$ , capacitance  
 $\theta$ , rotation angle  
 $V$ , voltage potential  
 $T_m$ , mechanical torque  
 $k_m$ , spring constant  
 $PI(\theta)$ , pull-in function  
 $\theta_{pi}$ , pull-in angle  
 $V_{pi}$ , pull-in voltage  
 $P(\theta)$ , coefficients of polynomial fit function  
 $r_i$ , length of linkage  $i$  in four-bar analysis  
 $L$ , length of beam  
 $a$ , thickness of rectangular beam cross-section  
 $b$ , width of rectangular beam cross-section  
 $K$ , cross-sectional term  
 $G$ , shear modulus  
 $F_i$ , force at joint  $i$

$T_{Si}$ , torque at joint  $i$   
 $\theta_{Si}$ , angle of joint  $i$   
 $\theta_{Si0}$ , initial angle of joint  $i$

## ELECTROSTATIC ANALYSIS

For the electrostatic comb drive mirror presented here, there is a ground plane and a series of vertically offset comb fingers, all contained underneath a flat mirror surface. A voltage potential is applied across the fixed fingers and the moving fingers of the device creating an electrostatic force. This force causes the mirror to rotate about an axis supported by the hidden spring suspension, shown separately in Figure 1(a). Not depicted in the drawing is a design constraint that restricts the motion in the  $z$  direction. While some motion may occur, the assumption is made that this device acts in one degree-of-freedom by rotating about the  $x$ -axis.

Because of the symmetry of the comb fingers, it is convenient to consider only one unit cell when calculating the capacitance of the device. A cross-section of a unit cell made up of one moving comb finger and one half of each associated fixed comb finger is shown in Figure 1(c). The electrostatic torque,  $T_e$ , may be represented by the following [5],

$$T_e = N \frac{1}{2} \frac{\partial C}{\partial \theta} V^2 \quad (1)$$

where  $C$  is the capacitance of one unit cell,  $\theta$  is the angle of rotation about the  $x$ -axis,  $V$  is the voltage potential, and  $N$  refers to the number of unit cells in the device.

It is assumed that the spring suspension provides a linear mechanical restoring torque,  $T_m$ , to the system that can be represented as [5],

$$T_m = k_m \theta \quad (2)$$

where  $k_m$  is the rotational spring constant. For this device,  $k_m$  was found to be approximately 75.79 pN- $\mu$ m/rad using beam4 elements in an Ansys finite element simulation.

Equilibrium occurs in the device when the electrostatic torque is equal to the mechanical restoring torque. When the electrostatic torque exceeds the ability of the mechanical spring, equilibrium can no longer be maintained and electrostatic pull-in occurs. At the pull-in point, both the electrostatic and mechanical torques are equal in magnitude and slope. Hah, et al. [5] derived analytical relationships to determine the pull-in angle and voltage. Equations (3)-(5) are only valid assuming that the restoring springs are linearly deformed in the range of actuation. The pull-in can be described by

$$\left(\frac{\partial C}{\partial \theta}\right)_{\theta=\theta_{PI}} - \theta_{PI} \left(\frac{\partial^2 C}{\partial \theta^2}\right)_{\theta=\theta_{PI}} = 0 \quad (3)$$

where  $\theta_{PI}$  is the pull-in angle. Based on the spring linearity assumption, the pull-in angle is independent of the spring stiffness. A pull-in function,  $PI(\theta)$ , is defined to determine the pull-in angle, which occurs when  $PI(\theta)$  is equal to zero.

$$PI(\theta) = \left(\frac{\partial C}{\partial \theta}\right) - \theta \left(\frac{\partial^2 C}{\partial \theta^2}\right) \quad (4)$$

In turn, once the pull-in angle is determined, the pull-in voltage can be calculated by the following expression,

$$V_{PI} = \sqrt{\frac{2k_m \theta_{PI}}{\left(\frac{\partial C}{\partial \theta}\right)_{\theta=\theta_{PI}}} \quad (5)$$

In order to evaluate the pull-in function and calculate the electrostatic torque of the device, the capacitance must be determined as a function of the rotation angle. Because of the complex geometry of the vertical comb drives, this may be done using a 3-D finite element analysis in ANSYS of one unit cell. The results of this analysis are plotted in Figure 2 along with a fourth order polynomial approximation of the data. The coefficients for the polynomial curve fit were found using the poly-fit command in MATLAB. The curve fit equation gives an approximation of the capacitance as a function of rotation angle.

$$C(\theta) = P(1)\theta^4 + P(2)\theta^3 + P(3)\theta^2 + P(4)\theta + P(5) \quad (6)$$

where the coefficients of the polynomial are

$$P = [0.0442 \ -0.0322 \ 0.0071 \ 0.0004 \ 0.0006].$$

The square of the residuals, or  $R^2$  value, for this fit is 0.9997, indicating it is a good estimate of the data. In order to determine an expression for  $\frac{\partial C}{\partial \theta}$ , the derivative of equation (6) is taken. This expression and its derivative may be used in the above equations to determine the electrostatic characteristics of the device. A plot of the pull-in function is shown in Figure 3 and pull-in occurs where the function equals zero at 16.5 degrees. Using this value in equation (5), the pull-in voltage is 46.73 volts.

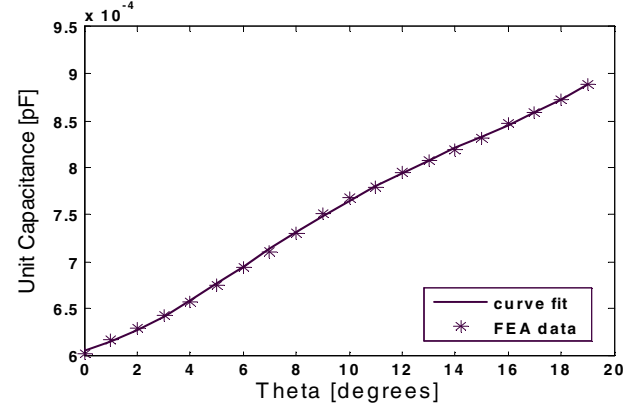


**Figure 2. Capacitance calculation as a function of rotation angle, theta, calculated using FEA data and a polynomial curve fit.**

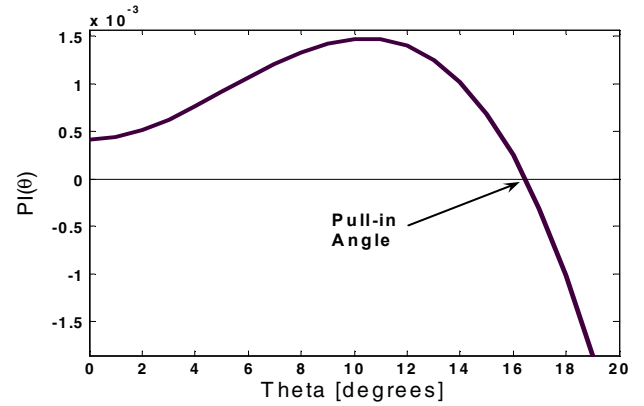


**Figure 3. Plot of the Pull-in function  $PI(\theta)$  showing that pull-in occurs at 16.5 degrees.**

Now that a relationship for the capacitance is known, the electrostatic torque in equation (1) can be calculated. The electrostatic torque is a function of the capacitance and voltage only, and therefore equation (1) holds true for the system regardless of the spring configuration. Figure 4 shows the electrostatic torque as a function of rotation angle for different values of voltage ranging from 10 volts to 100 volts. The straight line on the plot corresponds to the mechanical restoring torque of the spring from equation (2). There is a point at which this line runs tangent to the electrostatic torque, and this indicates the electrostatic pull-in point. Pull-in will happen at a rotation angle of 16.5°, and a voltage of 46.73 volts, agreeing with the results calculated from equations (4) and (5) respectively.

To further illustrate the ideas of equilibrium and pull-in, two cases are considered. The first case is an equilibrium point, marked on Figure 4 as point “A”. Here, for an input voltage of approximately 32 V, the mirror will maintain a static rotation of 10 degrees. The second case occurs after the pull-in point at 18 degrees and is marked on Figure 4 as point

“B”. However, this point cannot physically be achieved because the mirror has already been rotated to its final, fully-actuated position of 19 degrees due to the electrostatic torque being greater than the available mechanical restoring torque.

If the characteristics of the mechanical restoring force can be altered such that this pull-in never occurs, then the device could operate continuously over its full range of motion from 0 to 19 degrees. The following analysis proposes a new design for the spring that has a nonlinear restoring force such that the stiffness characteristics increase significantly as the spring is rotated. Such a design will be referred to as a progressive linkage.

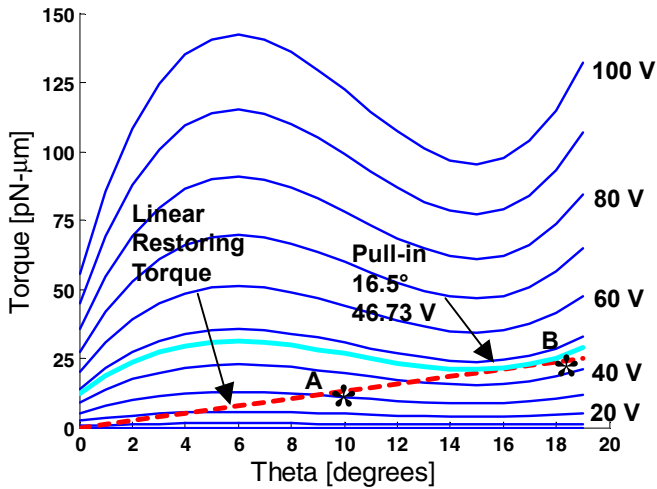


Figure 4. Torque as a function of rotation angle, theta, and voltage determined from equation (1) for different voltage values.

**PROGRESSIVE LINKAGE DESIGN**

The analysis for this design is based on an equivalent four-bar model as depicted in Figure 5. The geometric relationships between the links are shown in Figure 5(a). The kinematics of the mechanism can be denoted by the following vector sum where the vectors denote the position and orientation of each side of the mechanism shown in Figure 5.

$$\vec{r}_2 = \vec{r}_0 + \vec{r}_1 - \vec{r}_3 \tag{7}$$

Since the four-bar mechanism is a one-degree-of-freedom device, the angles  $\theta_2$  and  $\theta_3$  can be described as a function of  $\theta_1$ . That is, the length and orientation of each side can be used to determine the relationships of the angles  $\theta_2$  and  $\theta_3$ . By using the y and z components of the vector  $\vec{r}_2$ , an expression for  $\theta_2$  is given as

$$\theta_2 = \tan^{-1} \left( \frac{r_{2z}}{r_{2y}} \right) \tag{8}$$

In order to determine the angle  $\theta_3$ , begin with the relationship

$$r_2^2 = r_d^2 + r_3^2 - 2r_3r_d \cos \gamma_3 \tag{9}$$

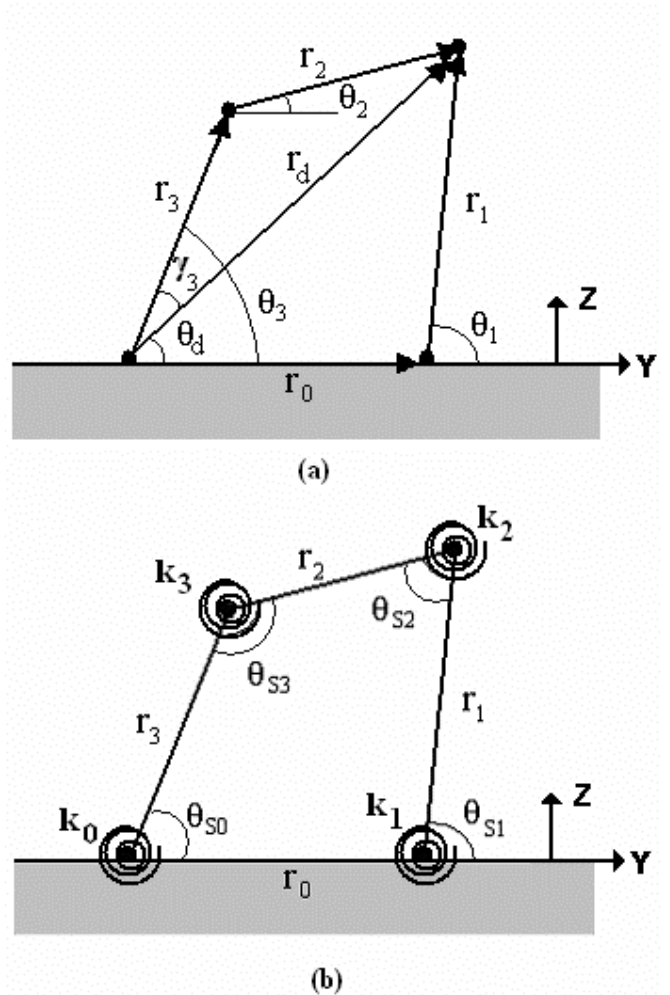
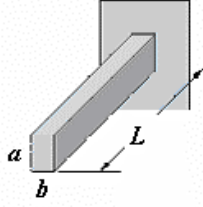


Figure 5. Diagram of four-bar mechanism for progressive linkage analysis showing (a) vectors and geometry and (b) springs for force and moment analysis.



**Figure 6.** The joints of the four-bar can be treated as cantilever beams of length  $L$ .

An expression for  $\theta_d$  is found from

$$\theta_d = \tan^{-1} \left( \frac{r_{0z} + r_{1z}}{r_{0y} + r_{1y}} \right) \quad (11)$$

The angle  $\theta_3$  is given as

$$\theta_3 = \theta_d + \gamma_3. \quad (12)$$

To realize this design scheme in a surface micromachined device, the design will be subject to the limits and constraints of the micromachining process. Assuming that this 2-D representation of the four-bar linkage is created using a series of thin beams, kinematically spaced by  $r_i$  ( $i = 0,1,2,3$ ), each joint may be considered as a beam in torsion that provides a restoring force to the system. A beam of length  $L$  with a rectangular cross-section, as shown in Figure 6, is used to model the stiffness at the joints. The restoring torque on the member can be calculated by

$$T_{s,i} = \frac{K_i(\theta_{s,i} - \theta_{s,i0})G}{L} \quad (15)$$

for each joint  $i = 0, 1, 2, 3$ , where  $G$  is the shear modulus and  $K_i$  are given as

$$K_i = \frac{ab^3}{16} \left[ \frac{16}{3} - 3.36 \frac{b}{a} \left( 1 - \frac{b^4}{12a^4} \right) \right]. \quad (16)$$

The resulting static force and moment equations can be determined from the free body diagrams in Figure 7.

$$\sum \bar{F}_{bar1} = \bar{F}_1 + \bar{F}_2 = 0 \quad (17)$$

$$\sum \bar{F}_{bar2} = -\bar{F}_2 + \bar{F}_3 = 0 \quad (18)$$

$$\sum \bar{F}_{bar3} = -\bar{F}_3 + \bar{F}_0 = 0 \quad (19)$$

$$\sum \bar{M}_{joint1} = \bar{T}_{S1} - \bar{T}_e + \bar{T}_{S2} + \bar{r}_1 \times \bar{F}_2 = 0 \quad (20)$$

$$\sum \bar{M}_{joint2} = -\bar{T}_{S2} + \bar{T}_{S3} - \bar{r}_2 \times \bar{F}_2 = 0 \quad (21)$$

$$\sum \bar{M}_{joint3} = \bar{T}_{S0} - \bar{T}_{S3} - \bar{r}_3 \times \bar{F}_0 = 0 \quad (22)$$

The relationships above combine to determine the torque output for a progressive linkage design.

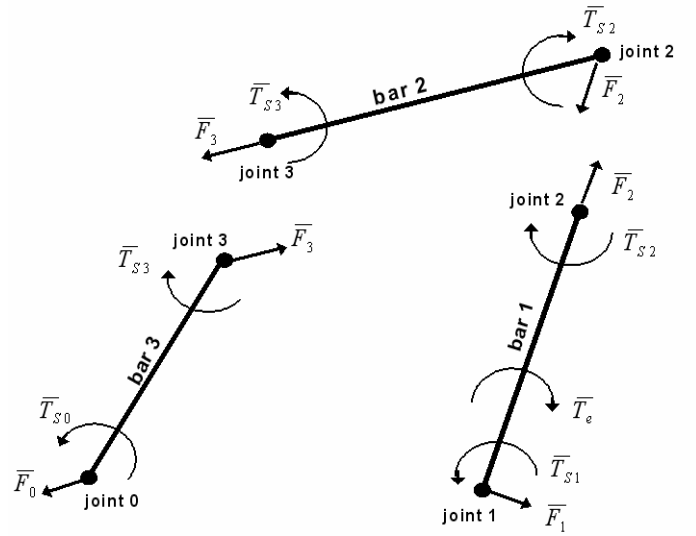


**Figure 7.** Free body diagrams for each member of the linkage.

## DESIGN IMPLEMENTATION

In order to realize the four-bar equivalent approach in a 3-D surface micromachined device, the design is greatly affected by the layers available in the surface micromachining process. The polysilicon layer thicknesses in SUMMIT™ V are shown in Figure 8. The layers are separated by sacrificial oxide, not shown [7]. The layer thicknesses will in part determine the cross-sectional area of the beams. A schematic of the proposed progressive linkage design is shown in Figure 9. This implementation of the four-bar design includes flexible beam members, and it is as yet unclear how the bending of these members will affect the device performance.

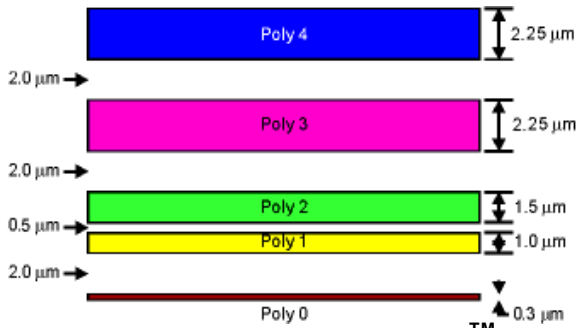


**Figure 8. Polysilicon layers in SUMMiT™ V surface micromachining separated by sacrificial oxide layers.**

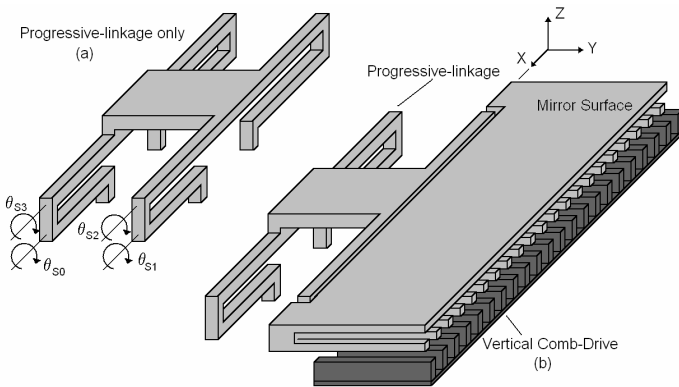
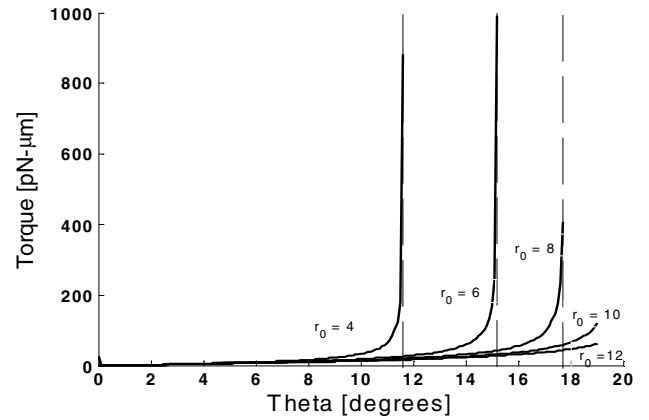


**Figure 9. Schematic of progressive linkage (a) by itself and (b) attached to mirror device.**

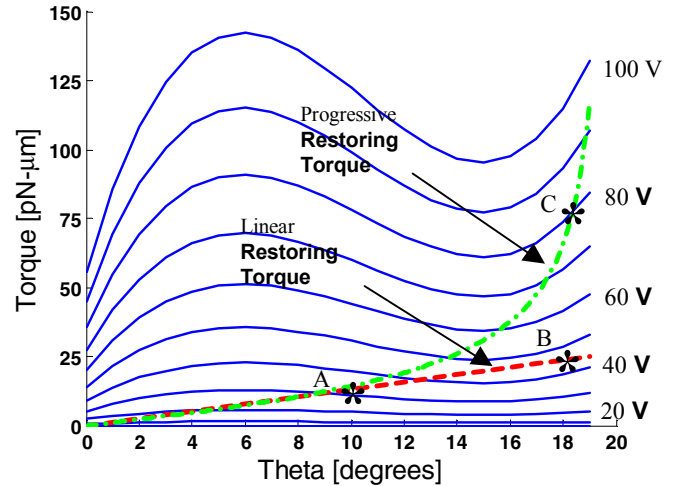
The dimension of the mechanism that is the easiest to change is the horizontal distance separating the anchor points of the device, referred to above as  $\bar{r}_0$ . Because of the planar fabrication requirements of surface micromachining, the diagonal top member of the four-bar device,  $\bar{r}_2$ , can be acquired via a kinematically equivalent L-shaped beam.

Figure 10 shows the output of the progressive linkage for different values of  $r_0$ . For a value of  $r_0$  less than 10  $\mu\text{m}$ , the structure will be very stiff and the mirror will not be able to fully rotate. This is seen for values of  $r_0$  equal to 4, 6, and 8  $\mu\text{m}$ . As the value of  $r_0$  is increased, the structure becomes more compliant. Figure 11 shows plots of the behavior of the progressive linkage for  $r_0$  equal to 10  $\mu\text{m}$  overlaying the electrostatic torque curves from Figure 4. The linear restoring force from Figure 4 is also included for comparison. The progressive linkage behavior does not at any point run tangent to the electrostatic torque curves, and therefore does not exhibit pull-in behavior. As before, point “A” is shown on the plot to represent an equilibrium point for both springs at 10 degrees and approximately 32 volts. Point “B”, which occurs

after the pull-in point, shows that a static rotation of 18 degrees is physically unattainable for the linear spring design. As a comparison for the progressive linkage design, point “C” represents static equilibrium 18 degrees. The progressive linkage is able to achieve static equilibrium for the full range of motion. The cost of this extended actuation range is that larger voltages are required.



**Figure 10. Progressive-linkage behavior for different values of  $r_0$  in  $\mu\text{m}$ .**



**Figure 11. Progressive linkage output for  $r_0$  equal to 10  $\mu\text{m}$  along with the electrostatic torque curves and the linear restoring torque.**

## CONCLUSIONS

The analysis presented here identifies the torque characteristics of a one-degree of freedom vertical comb drive mirror as a function of rotation about its axis. The current design with a linear restoring force is predicted to experience

pull-in at 16.5°, thus losing a portion of its full scanning range of 0 to 19 degrees. From this information, a progressive-linkage is designed to create a mechanical restoring force on the system that does not suffer from pull-in. The proposed design is based on a four-bar mechanism in which each joint has stiffness characteristics. A series of these designs are currently being fabricated in the SUMMiT™ V process at Sandia National Laboratories. Future work includes finite element model validation for this proposed design, experimental testing, and examining the ability of the progressive linkage to eliminate hysteresis associated with electrostatic instability.

#### ACKNOWLEDGMENTS

This work was supported by the United States Department of Energy under Contract DE-AC04-94AL85000. Sandia is a multiprogram laboratory operated by Sandia Corporation, a Lockheed Martin Company, for the United States Department of Energy.

#### REFERENCES

1. D. Hah, S.T. Huang, J-C. Tsai, H. Toshiyoshi, and M.C. Wu, "Low-Voltage, Large-Scan Angle MEMS Analog Micromirror Arrays with Hidden Vertical Comb-Drive Actuators", *Journal of Microelectromechanical Systems*, Vol. 3, No. 2, April 2004, pp. 279-289.
2. D. Hah, P.R. Patterson, H.D. Nguyen, H. Toshiyoshi, and M.C. Wu, "Theory and Experiments of Angular Vertical Comb-Drive Actuators for Scanning Micromirrors", *IEEE Journal of Selected Topics in Quantum Electronics*, Vol. 10, No. 3, May/June 2004, pp. 505-513.
3. J. Kim, and L. Lin, "A MEMS Tunable Capacitor Based on Plastically Deformed Vertical Comb Sets", *Proceedings of 2004 ASME International Mechanical Engineering Congress and Exposition*, Nov. 13-20, Anaheim, CA.
4. W.C. Tang, M.G. Lim, and R.T. Howe, "Electrostatic Comb Drive Levitation and Control Method", *Journal of Microelectromechanical Systems*, Vol. 1, No. 4, Dec. 1992, pp. 170-178.
5. D. Hah, H. Toshiyoshi, and M.C. Wu, "Design of Electrostatic Actuators for MOEMS Applications", *Design, Test, Integration and Packaging of MEMS/MOEMS 2002, Proceedings of SPIE*, Vol. 4755, pp. 200-207.
6. S-J. J. Lee, R.K. Yee, R. Kelley, R. Martin, A. Sadaka, and T-R. Hsu, "A Monolithic Micro Four-Bar Mechanism with Flexure Hinges", *Proceedings of 2004 ASME International Mechanical Engineering Congress and Exposition*, Nov. 13-20, Anaheim, CA.
7. Sandia National Laboratories, <http://www.sandia.gov/mstc/technologies/micromachines/techinfo/technologies/summit5.html>, February 10, 2005.